

X-RAY AND OPTICAL STUDY OF THE GAMMA-RAY SOURCE 3FGL J0838.8–2829: IDENTIFICATION OF
A CANDIDATE MILLISECOND PULSAR BINARY
AND AN ASYNCHRONOUS POLAR

JULES P. HALPERN¹, SLAVKO BOGDANOV¹, AND JOHN R. THORSTENSEN²
(Received 2016 November 8; Accepted 2017 January 13)

ABSTRACT

We observed the field of the *Fermi* source 3FGL J0838.8–2829 in optical and X-rays, initially motivated by the cataclysmic variable (CV) 1RXS J083842.1–282723 that lies within its error circle. Several X-ray sources first classified as CVs have turned out to be γ -ray emitting millisecond pulsars (MSPs). We find that 1RXS J083842.1–282723 is in fact an unusual CV, a stream-fed asynchronous polar in which accretion switches between magnetic poles (that are $\approx 120^\circ$ apart) when the accretion rate is at minimum. High-amplitude X-ray modulation at periods of 94.8 ± 0.4 minutes and 14.7 ± 1.2 hr are seen. The former appears to be the spin period, while the latter is inferred to be one-third of the beat period between the spin and the orbit, implying an orbital period of 98.3 ± 0.5 minutes. We also measure an optical emission-line spectroscopic period of 98.413 ± 0.004 minutes, which is consistent with the orbital period inferred from the X-rays. In any case, this system is unlikely to be the γ -ray source. Instead, we find a fainter variable X-ray and optical source, XMMU J083850.38–282756.8, that is modulated on a time scale of hours in addition to exhibiting occasional sharp flares. It resembles the black widow or redback pulsars that have been discovered as counterparts of *Fermi* sources, with the optical modulation due to heating of the photosphere of a low-mass companion star by, in this case, an as-yet undetected MSP. We propose XMMU J083850.38–282756.8 as the MSP counterpart of 3FGL J0838.8–2829.

Subject headings: cataclysmic variables — gamma rays: stars — pulsars: general — X-rays: individual (1RXS J083842.1–282723, XMMU J083850.38–282756.8, XMMU J083842.85–282831.8)

1. INTRODUCTION

The Large Area Telescope on the *Fermi* Gamma-ray Observatory has detected numerous young pulsars, as well as recycled millisecond pulsars (MSPs) in close binary systems. Most prominent of the new discoveries are the black widow (BW) pulsars and so-called “redback” systems (Roberts 2013), which comprise a large fraction of the MSPs selected by *Fermi*. The BWs are MSPs with sub-stellar mass, degenerate companions, while the redbacks generally have $> 0.1 M_\odot$ evolved companions. The latter are usually close to filling their Roche-lobes, which makes them a direct link to the low-mass X-ray binary (LMXB) progenitors of MSPs.

Recently, three redbacks have been observed to transition between radio pulsar and accreting states on timescales of years: PSR J1023+0038 (Archibald et al. 2009), XSS J12270–4859 (Roy et al. 2015), and PSR J1824–2452I in the globular cluster M28 (Papitto et al. 2013). All of these are hard X-ray and/or γ -ray sources. PSR J1023+0038 was initially misclassified as a cataclysmic variable (CV) (Bond et al. 2002, but see Thorstensen & Armstrong 2005 for a contrary interpretation), as was XSS J12270–4859 (Masetti et al. 2006; Butters et al. 2008), because of the similarity of their optical emission-line spectra and luminosities to those of CVs. Now we know that transitional MSPs are distinguishable from CVs by their X-ray and optical light curves,

which show characteristic dips and flares that are unique to this class (Bogdanov et al. 2015; de Martino et al. 2013). We employed this test to reevaluate two *ROSAT* All-Sky Survey X-ray sources in *Fermi* error circles that were spectroscopically classified as CVs by Masetti et al. (2013). Using X-ray and optical time-series data for one of these, 1RXS J154439.4–112820/3FGL J1544.6–1125, we concluded that it is almost certainly an MSP binary in the accreting state (Bogdanov & Halpern 2015). Here, we report on a similar investigation of the second Masetti et al. CV, 1RXS J083842.1–282723 in the error circle of 3FGL J0838.8–2829 (Acero et al. 2015).

Section 2 describes the observations obtained. Section 3 presents the results of optical and X-ray observations of 1RXS J083842.1–282723, which show that it is indeed a CV, probably an asynchronous polar (AM Hercules star). Section 4 reports the discovery of a second X-ray and optical source in the *Fermi* error circle, XMMU J083850.38–282756.8, which we identify as a candidate BW pulsar system, and likely the counterpart of the γ -ray source. In Section 5 we show that a third X-ray source in the *Fermi* error circle is a QSO, probably unrelated to the γ -ray source. Section 6 discusses the properties of the CV and the MSP candidate in relation to other objects in their respective classes.

2. X-RAY AND OPTICAL OBSERVATIONS

The field of 3FGL J0838.8–2829 was observed twice with *XMM-Newton*, on 2015 October 20 (ObsID 0764420101, 53 ksec) and 2015 December 2 (ObsID 0790180101, 77 ksec). The EPIC pn detector was used in large window mode, while the two MOS detectors were

¹ Columbia Astrophysics Laboratory, Columbia University, 550 West 120th Street, New York, NY 10027-6601; jules@astro.columbia.edu

² Department of Physics and Astronomy, 6127 Wilder Laboratory, Dartmouth College, Hanover, NH 03755-3528

TABLE 1
LOG OF MDM OBSERVATORY TIME-SERIES PHOTOMETRY OF 1RXS J083842.1–282723

Telescope/Detector	Date (UT)	Time (TDB)	Filter	Exposure (s)	Conditions
2.4 m/Templeton	2014 Mar 22	02:47–06:47	V	10	Clear
2.4 m/Templeton	2014 Mar 23	02:40–06:51	V	10	Photometric
1.3 m/Templeton	2015 Feb 17	06:12–09:19	BG38	20	Partly cloudy
1.3 m/Templeton	2015 Feb 18	03:51–09:14	BG38	20	Photometric
1.3 m/Andor	2016 Mar 16	04:31–06:31	GG420	5	Photometric
1.3 m/Andor	2016 Mar 17	04:02–06:02	GG420	5	Photometric

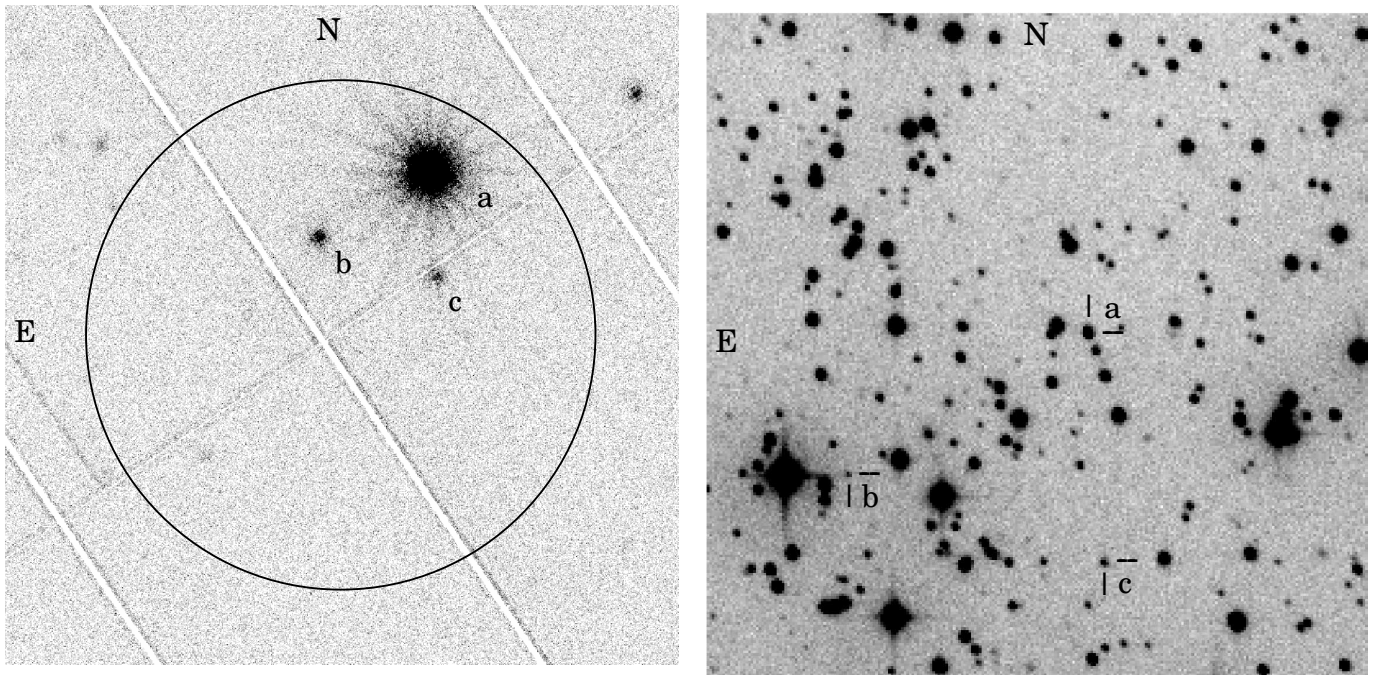


FIG. 1.— Left: *XMM-Newton* EPIC pn image (0.3–10 keV) from 2015 December 2 (ObsID 0790180101) showing the *Fermi* error circle of 3FGL J0838.8–2829 with a 95% confidence radius of $3'.6$. Right: Finding chart from an MDM 1.3m image taken through a BG38 filter. The field is $4'.3 \times 4'.3$. Labeled sources in both images are (a) the CV 1RXS J083842.1–282723, (b) the MSP candidate XMMU J083850.38–282756.8, and (c) the QSO XMMU J083842.85–282831.8.

TABLE 2
OPTICAL POSITIONS

Label	Source	R.A. (h m s)	Decl. ($^{\circ}$ ' ")
a	1RXS J083842.1–282723	08 38 43.34	–28 27 00.9
b	XMMU J083850.38–282756.8	08 38 50.45	–28 27 57.4
c	XMMU J083842.85–282831.8	08 38 42.80	–28 28 31.0

NOTE. — Coordinates are equinox J2000.0

configured in small window mode, all with the thin filter. Time resolution is 48 ms for the pn, and 0.3 s for the MOS. In addition, the *XMM-Newton* Optical Monitor (OM) obtained 10 contemporaneous exposures of 5000 s or 4160 s in the *V*-band on 2015 October 20, and 15 contemporaneous 4400 s exposures in the *B*-band on 2015 December 2. Figure 1 (left) shows the *Fermi* 95% error circle superposed on the *XMM-Newton* pn image of 2015 December 2. In addition to 1RXS J083842.1–282723 (source “a”), there are two fainter sources inside the error circle that we investigated, labeled “b” and “c”. The MOS small window only included source “a”, but all

three sources have optical counterparts in the OM images.

We obtained another X-ray observation of 1RXS J083842.1–282723 using *Chandra* ACIS on 2016 July 7 for an exposure time of 30 ks (ObsID 17769). The S3 CCD only was operated in continuous clocking (CC) mode to avoid pileup of the bright source 1RXS J083842.1–282723. This gives time resolution of 2.85 ms, but sacrifices one spatial dimension. Only 1RXS J083842.1–282723 is bright enough to study in CC mode.

We obtained several hours of time-series optical photometry of the field using the MDM Observatory 1.3m and 2.4m telescopes on Kitt Peak during three observing runs in 2014, 2015, and 2016. The detectors used were either the 1024×1024 pixel thinned, back-illuminated SITE CCD “Templeton,” or a thermoelectrically cooled Andor Ikon DU-937 N CCD camera. The detectors, observing parameters, and differential photometry techniques were the same as described in Thorstensen & Halpern (2013) and Halpern & Thorstensen (2015). The CCD readout was windowed and binned to reduce dead-time. Exposure times were 10 s or 20 s, with 3 s dead-time using

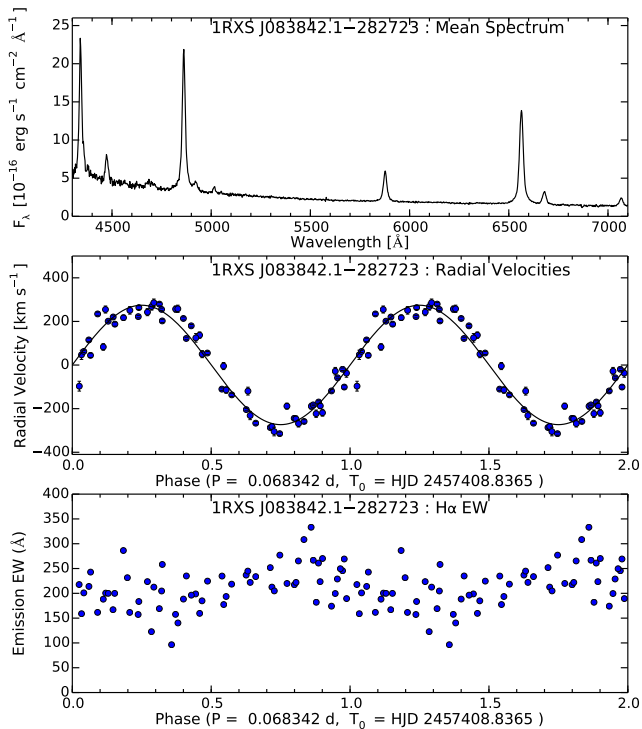


FIG. 2.— Top: Mean spectrum of 1RXS J083842.1–282723. Middle: Radial velocities of the H α emission line, folded on the best-fitting period, together with a sinusoidal fit. The error bars shown are based on signal-to-noise and do not include systematic effects. The data are repeated for a second cycle for continuity. Bottom: Equivalent width of the H α emission line.

Templeton, and 5 s exposures with 12 ms dead-time using the Andor. A log of the observations is given in Table 1. The 1.3m Templeton images (Figure 1, right) covered all three X-ray sources, while the Andor and 2.4m Templeton images only included 1RXS J083842.1–282723. Optical positions for the three sources, measured from a 1.3m image using USNO B1.0 catalog stars for the astrometric solution, are given in Table 2.

We obtained 59 spectra of 1RXS J083842.1–282723 during two observing runs, in 2016 January and February, using the 2.4m telescope with the modular spectrograph and a thinned, back-illuminated 2048×2048 pixel SiTe CCD detector. Our spectra covered 4210–7500 \AA , with $2.0 \text{ \AA pixel}^{-1}$ and a FWHM resolution of $\approx 3.5 \text{ \AA}$. The observing, reduction, and analysis protocols were practically identical to those used in Thorstensen & Halpern (2013) and Halpern & Thorstensen (2015). A log of the spectroscopic observations is given in Table 3. Finally, we obtained one identification spectrum of source ‘c’ using the Ohio State Multi-Object Spectrograph (OSMOS) on the 2.4m.

3. 1RXS J083842.1–282723

3.1. Optical Spectroscopy

Our mean spectrum of 1RXS J083842.1–282723 (Figure 2, upper panel) appears similar to that published by Masetti et al. (2013), with strong, single-peaked Balmer and He I lines on a blue continuum. He II $\lambda 4686$ is just detected with an emission equivalent width (EW)

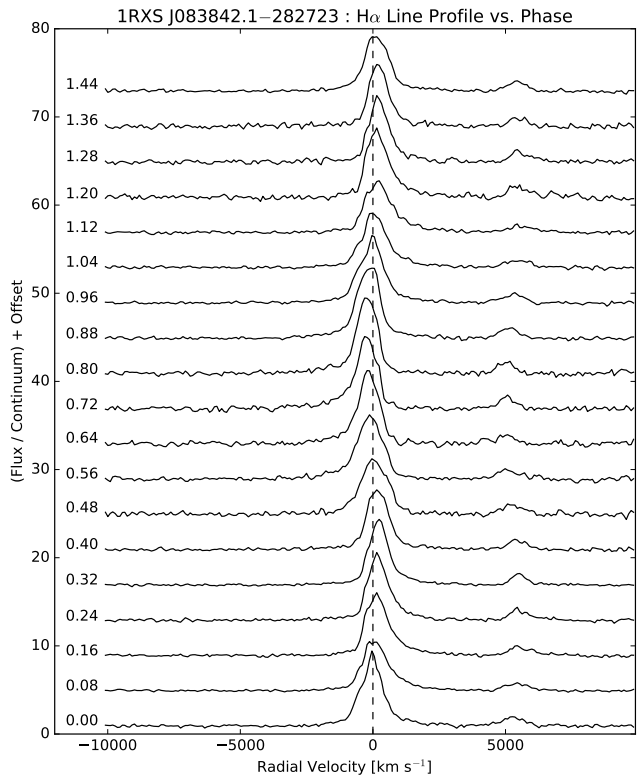


FIG. 3.— Rectified spectra of 1RXS J083842.1–282723 near H α , as a function of orbital phase. Each trace is a weighted average of spectra taken near the phase indicated. Successive traces have been shifted upward by four times the continuum.

of $\sim 8 \text{ \AA}$, but is much less prominent than H β (EW $\approx 125 \text{ \AA}$). The spectrum implies a synthetic $V \sim 18.0$, but this is not expected to be precise because of occasional clouds and poor seeing.

We measured radial velocities of H α using a convolution function tuned to be sensitive to the steep sides of the line profile, which are about 1500 km s^{-1} apart. Table 3 lists the resulting radial velocities and uncertainties. To find the period we constructed a dense grid of trial frequencies and fitted the velocities with least-squares sinusoids at each frequency. This yielded a period near 98.4 minutes, with no ambiguity in the daily or month-to-month cycle count. A least-squares best fit of the form $v_r(t) = \gamma + K \sin[2\pi(t - T_0)/P]$ has

$$T_0 = \text{BJD } 2457408.8365 \pm 0.0006 \quad (1)$$

$$P = 0.068342(3) \text{ d} \quad (2)$$

$$K = 274 \pm 16 \text{ km s}^{-1} \quad (3)$$

$$\gamma = 49 \pm 11 \text{ km s}^{-1} \quad (4)$$

with an RMS scatter of 36 km s^{-1} for the 59 data points. The precise period is 98.413 ± 0.004 minutes. The middle panel of Figure 2 shows the sine fit superposed on the radial velocities, and Figure 3 shows the H α line profiles as function of orbital phase.

The lower panel of Figure 2 shows the equivalent width (EW) of the H α emission line as a function of spectroscopic phase. A periodogram of the EW has a peak at exactly the spectroscopic period. Although noisy, the

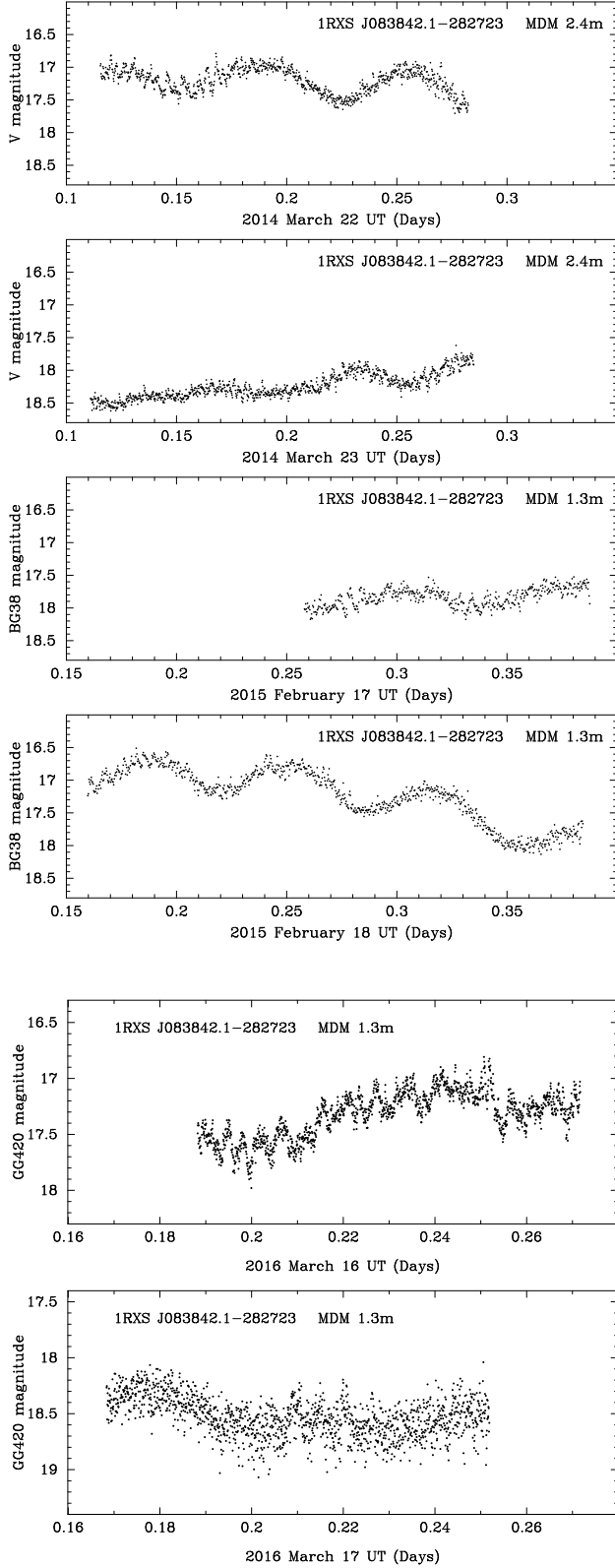


FIG. 4.— MDM light curves of 1RXS J083842.1–282723; the log of observations is given in Table 1. Times are barycentric dynamical time (TDB).

TABLE 3
H α SPECTROSCOPY OF 1RXS J083842.1–282723

Date (BJD) ^a	Exposure (s)	v_r (km s ⁻¹)	σ (km s ⁻¹)	H α EW (Å)
2457402.8178	900	-119	6	174
2457402.8286	900	234	8	162
2457403.8843	480	-110	6	235
2457403.8903	480	-204	6	237
2457403.8962	480	-287	7	252
2457403.9021	480	-244	6	217
2457403.9081	480	-170	6	261
2457403.9140	480	-19	6	246
2457403.9199	480	115	8	214
2457403.9259	480	220	9	167
2457405.7628	480	-97	23	218
2457405.7687	480	83	15	188
2457405.7806	480	268	16	123
2457405.7865	480	257	14	158
2457405.7924	480	137	15	160
2457405.7983	480	-5	16	177
2457405.8043	480	-120	18	245
2457405.8102	480	-282	14	213
2457405.8161	480	-247	13	222
2457405.8221	480	-187	12	224
2457405.8280	480	-101	9	269
2457405.8339	480	44	10	243
2457405.8399	480	188	9	200
2457405.8458	480	263	9	184
2457405.9192	480	279	8	169
2457405.9251	480	214	7	188
2457405.9310	480	55	7	225
2457405.9370	480	-137	7	219
2457405.9429	480	-267	8	234
2457405.9488	480	-315	7	277
2457405.9548	480	-259	8	308
2457407.7556	480	217	12	286
2457407.7615	480	243	16	224
2457407.7734	480	125	20	199
2457407.8030	480	-223	17	182
2457408.7526	480	-188	14	220
2457408.7586	480	-189	13	333
2457408.7645	480	-28	17	200
2457408.7704	480	47	21	159
2457408.7763	480	255	16	200
2457408.7823	480	251	17	162
2457408.7882	480	286	17	213
2457408.7941	480	258	17	140
2457408.8001	480	50	16	185
2457408.8060	480	-115	15	194
2457408.8119	480	-232	19	222
2457408.8178	480	-305	20	205
2457408.8238	480	-268	16	265
2457408.8297	480	-219	16	270
2457408.8356	480	-37	19	189
2457430.8336	480	-183	4	267
2457430.8396	480	-59	5	229
2457430.8455	480	62	5	201
2457430.8515	480	201	5	200
2457438.7866	480	222	6	157
2457438.7925	480	202	8	258
2457438.7984	480	122	6	235
2457440.8426	600	255	6	205
2457440.8499	600	180	6	196

^a Barycentric Julian day of mid-integration in the UTC system.

EW varies sinusoidally with a phase lag of ≈ 0.5 cycles with respect to the radial velocity curve. As will be discussed, this is a clue to the accretion geometry.

3.2. Time-series Optical Photometry

The MDM light curves of 1RXS J083842.1–282723 are shown in Figure 4. Magnitudes were calibrated to stars in the UCAC4 (Zacharias et al. 2013). BG38 and GG420

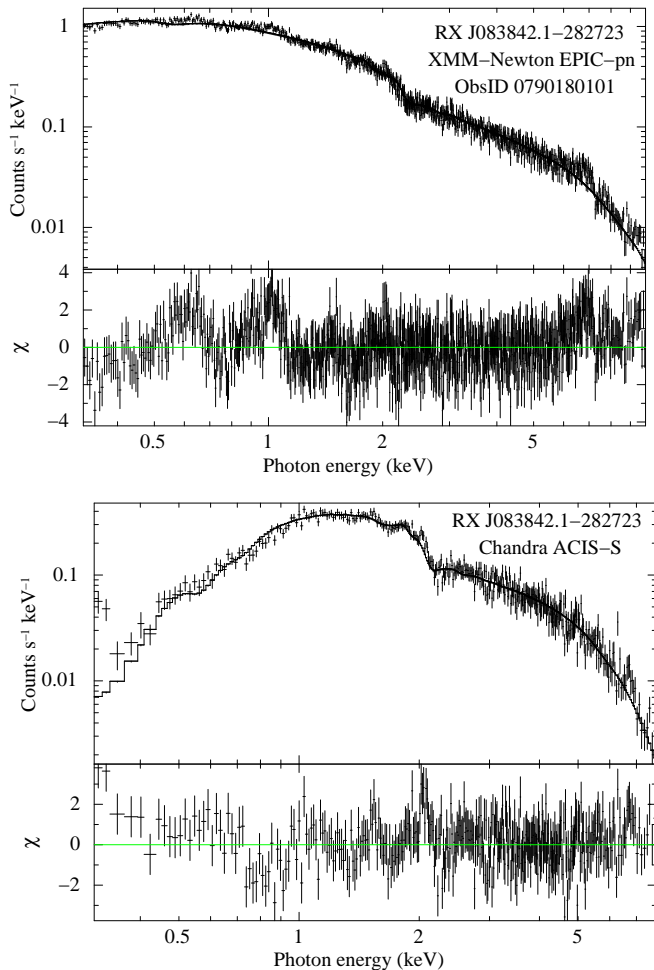


FIG. 5.— X-ray spectra of 1RXS J083842.1–282723 fitted to a thermal bremsstrahlung model. Parameters of the fit are listed in Table 4. Residuals correspond to Fe $K\alpha$ 6.7, 6.9 keV, as well as Fe L-shell (1 keV) and O K-shell (0.6 keV) emission lines from the hot plasma.

are broadband filters chosen for their higher throughput, but they do not have standard calibrations. We approximated their magnitudes using V and R , respectively, from stars in the UCAC4.

The individual time series all display a broad oscillation with a period of ~ 0.07 d, similar to the spectroscopic period. Although some of the light curves in Figure 4 show a hint of a faster oscillation, a power-spectrum analysis does not reveal any shorter coherent period. In addition, in all three years there is a large change of ≈ 1.5 magnitudes between adjacent nights. When the star is bright, the ~ 0.07 d oscillation has large amplitude; when it is faint the relative amplitude is smaller. This behavior matches the X-ray (presented in the next section) very well, with the night-to-night changes explained as modulation of the accretion rate on the beat period between the spin and the orbit of a stream-fed system.

3.3. XMM-Newton Analysis

We fitted the pn X-ray spectrum from the longer XMM-Newton observation with a thermal bremsstrahlung model in XSPEC. The temperature

is 11.7 keV (Figure 5 and Table 4), and residuals corresponding to Fe $K\alpha$ 6.7, 6.9 keV, as well as Fe L-shell and O K-shell lines, are evident. A mekal hot plasma model gives a similar temperature. There is no evidence of a soft blackbody from the white dwarf (WD) surface that is sometimes but not always seen in polars.

X-ray photon arrival times were transformed to Barycentric Dynamical Time and extracted from a $20''$ radius around 1RXS J083842.1–282723. Figures 6 and 7 show the 0.2–10 keV, background subtracted, combined light curve from the pn and MOS in 60 s bins, as well as magnitudes from the OM. The X-ray light curve shows a factor of 10 variation with a period of ≈ 0.07 d, as well as a broader modulation on a timescale of ~ 0.6 d. This resembles a classic beating between two closely spaced frequencies. A Z_1^2 periodogram of the longer (December 2) observation (Figure 8a) shows three peaks, at 88.0 minutes, 98.3 minutes, and 14.7 hr, where the latter is consistent with the beat between the two shorter periods. However, a periodogram of the shorter observation (October 20; Figure 8c) has only a single peak at a period of 95 minutes, which falls in between the pair at 88.0 minutes and 98.3 minutes.

Inspection of the light curves reveals what is responsible for the difference in the power spectra. At the minimum of the 14.7 hr cycle, the phase of the shorter period jumps by $\approx 120^\circ$. This is especially clear in Figure 7, where the periodic tick marks switch from marking flux minima before day 7360 to nearly flux maxima after day 7360. This phase jump causes the peak in the Fourier transform to split into two, straddling the true peak. By analogy with amplitude modulation of a carrier signal, one should still see the carrier in the power spectrum, with symmetric sidebands on either side. However, if the carrier (or any signal) experiences a phase jump, then its power will be split into two frequencies, neither of which is the true one. The frequency splitting of the signal should be equal to the frequency with which the phase jumps, in this case $1/14.7 \text{ hr}^{-1}$, which is consistent with the observed splitting of $1/14.0 \text{ hr}^{-1}$.

We tested this interpretation by measuring the power spectrum of the first part of the December 2 observation, before the minimum of the beat cycle at day 7360 in Figure 7. This restricted power spectrum has a single peak at 94.6 minutes (Figure 8b), consistent with the period from October 20. The same period is also confirmed in a Chandra observation described below. Therefore, we adopt the average value of 94.8 ± 0.4 minutes from the two XMM-Newton observations as the probable spin period of the WD.

We further confirm this interpretation using simulated light curves and power spectra. As an approximation of the light curve, a squared sinusoid with a 94.8 minute period was amplitude modulated at the 14.7 hr period, and a phase jump of varying angle was introduced at day 7360. This reproduced well the splitting of the spin signal in the observed power spectrum. The best match to the observed light curve and power spectrum was achieved for a phase jump of $\approx 120^\circ$, with an uncertainty of $\sim 20^\circ$.

We hypothesize that the WD spin modulates the apparent X-ray flux by self occultation of the base of a column that accretes onto a magnetic pole in an AM Her-like system. The 14.7 hr amplitude modulation su-

TABLE 4
X-RAY SPECTRAL FITS

Label	Source	N_{H} (cm^{-2})	kT_{br} (keV)	Γ	F_x (0.3–10 keV) ^a	χ^2_{ν} (dof)
<i>Chandra</i> ACIS-S, ObsID 17769, 2016 July 7						
a	1RXS J083842.1–282723	$5.6^{+1.5}_{-1.4} \times 10^{20}$	$11.2^{+1.3}_{-1.1}$...	$(9.43 \pm 0.14) \times 10^{-12}$	1.25 (368)
<i>XMM-Newton</i> EPIC-pn, ObsID 0790180101, 2015 December 2						
a	1RXS J083842.1–282723	$1.03^{+0.21}_{-0.20} \times 10^{20}$	11.7 ± 0.5	...	$(6.61 \pm 0.06) \times 10^{-12}$	1.48 (883)
b	XMMU J083850.38–282756.8	$1.19^{+0.37}_{-0.33} \times 10^{21}$...	1.5 ± 0.1	$(1.73 \pm 0.11) \times 10^{-13}$	0.96 (109)
b	XMMU J083850.38–282756.8	$(7.1 \pm 2.1) \times 10^{20}$	$14.4^{+11.1}_{-5.2}$...	$(1.63 \pm 0.13) \times 10^{-13}$	0.99 (109)
c	XMMU J083842.85–282831.8	$1.26^{+0.69}_{-0.59} \times 10^{21}$...	2.2 ± 0.3	$7.99^{+0.11}_{-0.08} \times 10^{-14}$	0.69 (44)

NOTE. — Uncertainties are 90% confidence.

^a Unabsorbed flux in units of $\text{erg cm}^{-2} \text{s}^{-1}$.

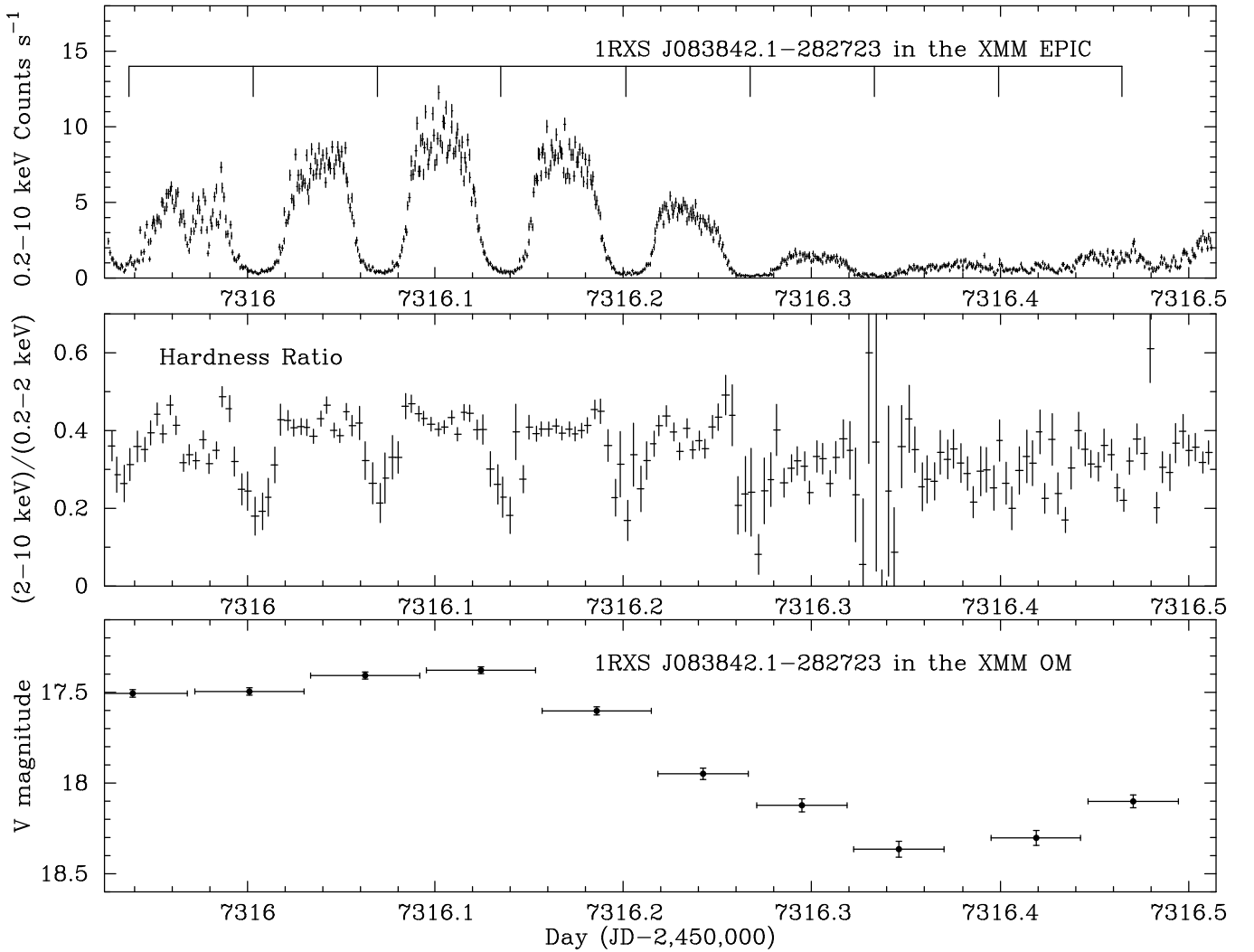


FIG. 6.— Background-subtracted *XMM-Newton* light curve of 1RXS J083842.1–282723 on 2015 October 20 (ObsID 0764420101). Top: Combined EPIC pn and MOS broad-band (0.2–10 keV) light curve in 60 s bins. The 95 minute period is indicated by tick marks, which reveal the $\approx 120^\circ$ phase jump after minimum light of the beat cycle. Middle: Hardness ratio of counts in the (2–10 keV)/(0.2–2 keV) bands, in 300 s bins. Bottom: *XMM-Newton* OM magnitudes from 5000 s or 4160 s exposures in the V-band.

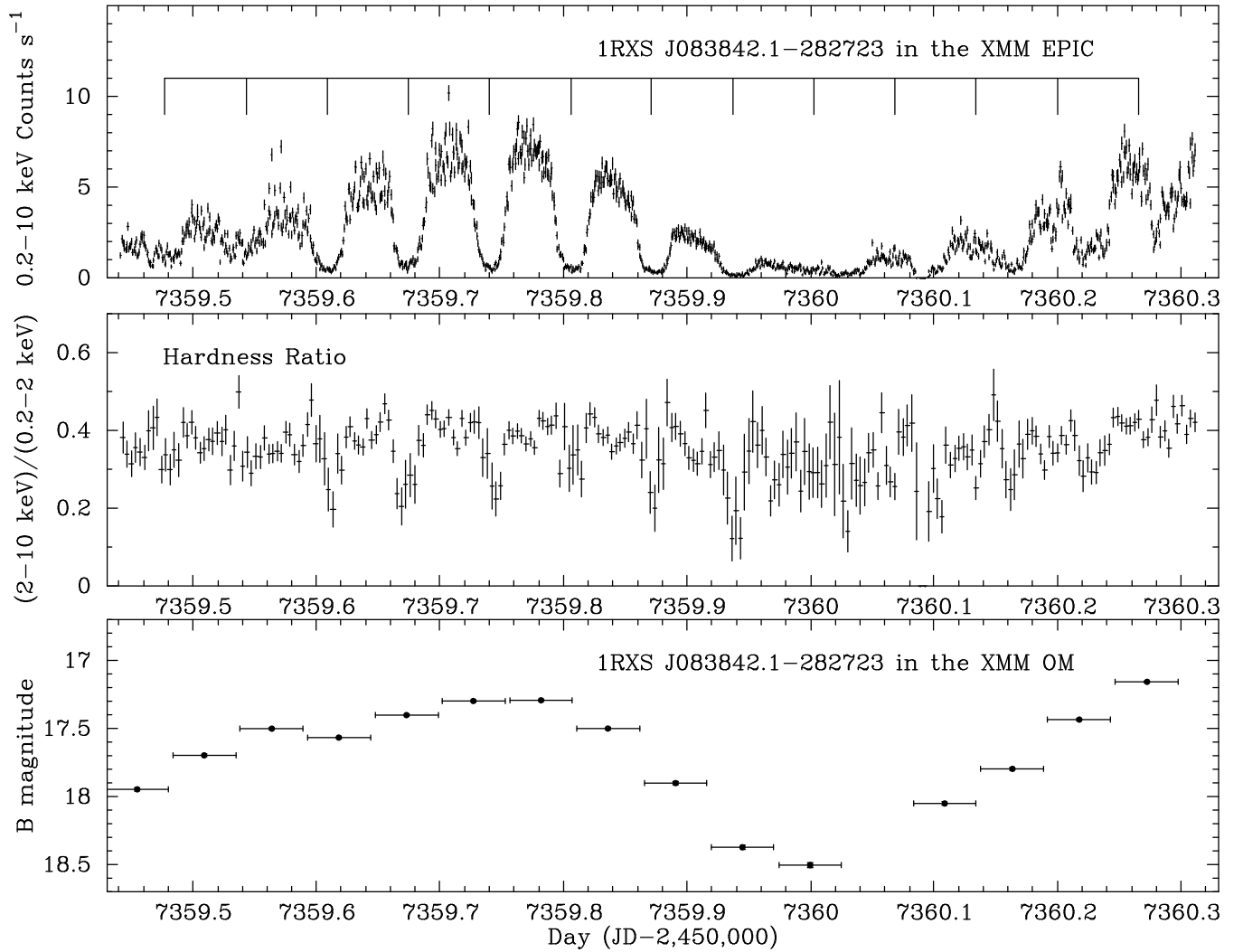


FIG. 7.— Background-subtracted *XMM-Newton* light curve of 1RXS J083842.1–282723 on 2015 December 2 (ObsID 0790180101). Top: Combined EPIC pn and MOS broad-band (0.2–10 keV) light curve in 60 s bins. There is a short gap in the data at day 7360.09. The 94.6 minute period is indicated by tick marks, which reveal the $\approx 120^\circ$ phase jump after minimum light of the beat cycle. Middle: Hardness ratio of counts in the (2–10 keV)/(0.2–2 keV) bands, in 300 s bins. Bottom: *XMM-Newton* OM magnitudes from 4400 s exposures in the *B*-band. There is a gap in the data at day 7360.05.

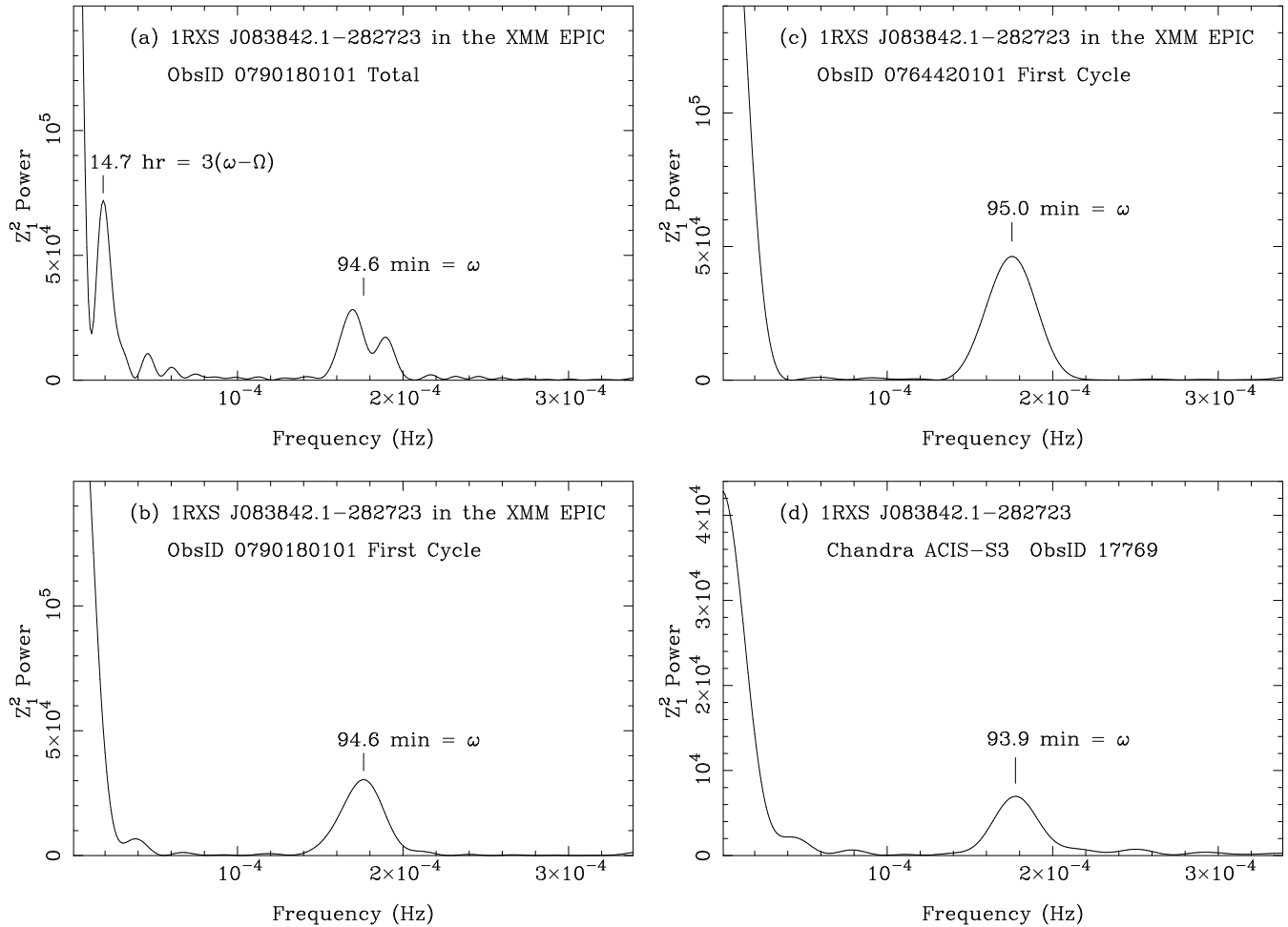


FIG. 8.— Power spectra of the X-ray light curves of 1RXS J083842.1-282723. (a) From the *XMM-Newton* observation of Figure 7, the 94.6 minute spin period is split into peaks at 98.3 minutes and 88.0 minutes by the phase jump after the minimum of the beat cycle at day 7360. The 14.7 hr period is inferred to be one-third of the beat cycle because the phase jump indicates that there is pole switching spanning $\approx 120^\circ$. The spin frequency is ω and the inferred orbital frequency is Ω . (b) When the power spectrum is restricted to the first beat cycle, before day 7360 in Figure 7, a single peak at the true period of 94.6 minutes is recovered. (c) The power spectrum of the *XMM-Newton* observation of Figure 6, restricted to the first beat cycle (before day 7316.4). The 95 minute period is consistent with the other X-ray observations. (d) The power spectrum of the *Chandra* observation of Figure 9, which does not span a minimum of the beat cycle. The 93.9 minute period is consistent with the other X-ray observations. We adopt 94.8 ± 0.4 minutes as the spin period.

perposed on this oscillation occurs as the secondary star migrates in the rotating frame of the WD. The $\approx 120^\circ$ phase jump of the 94.8 minute signal at the minimum of the beat cycle corresponds to switching of the accretion from one magnetic pole to the other. Evidently the accretion rate drops almost to zero during the switch. In this interpretation, 14.7 hours is one-third of the beat period between the spin and the orbit; therefore, the orbital period is 98.3 ± 0.5 minutes, if it is longer than the spin period. (Here we have estimated by eye from the light curve an uncertainty of ± 1.2 hr on the 14.7 hr period.) The 98.41 minute optical spectroscopic period is consistent with the orbital period deduced from the X-ray light curve.

The OM light curves in Figures 6 and 7, and MDM optical light curves in Figure 4, display these effects as well, with an amplitude that is smaller than the X-ray amplitude on the spin period, but similar to the X-ray amplitude on the beat period. This supports the hypoth-

esis that the emission is from an accretion stream rather than a disk. The optical light may be less modulated by the spin of the white dwarf than the X-rays, because it is coming from higher in the accretion column. But the varying accretion rate affects the X-ray and optical luminosity equally on the beat period.

Notably, the X-ray hardness ratio shown in Figures 6 and 7 becomes softer in the dips. This may indicate that a broader, warm area of emission is present that is occulted less completely than the central, hot base of the accretion column (see review by Wickramasinghe 1989). Alternatively, there may be residual luminosity from another accreting region that is cooler and less luminous.

3.4. Chandra Analysis

We fitted the *Chandra* X-ray spectrum with a thermal bremsstrahlung model in XSPEC, finding a temperature of 11.2 keV (Figure 5 and Table 4), consistent with the *XMM-Newton* results. X-ray photon ar-

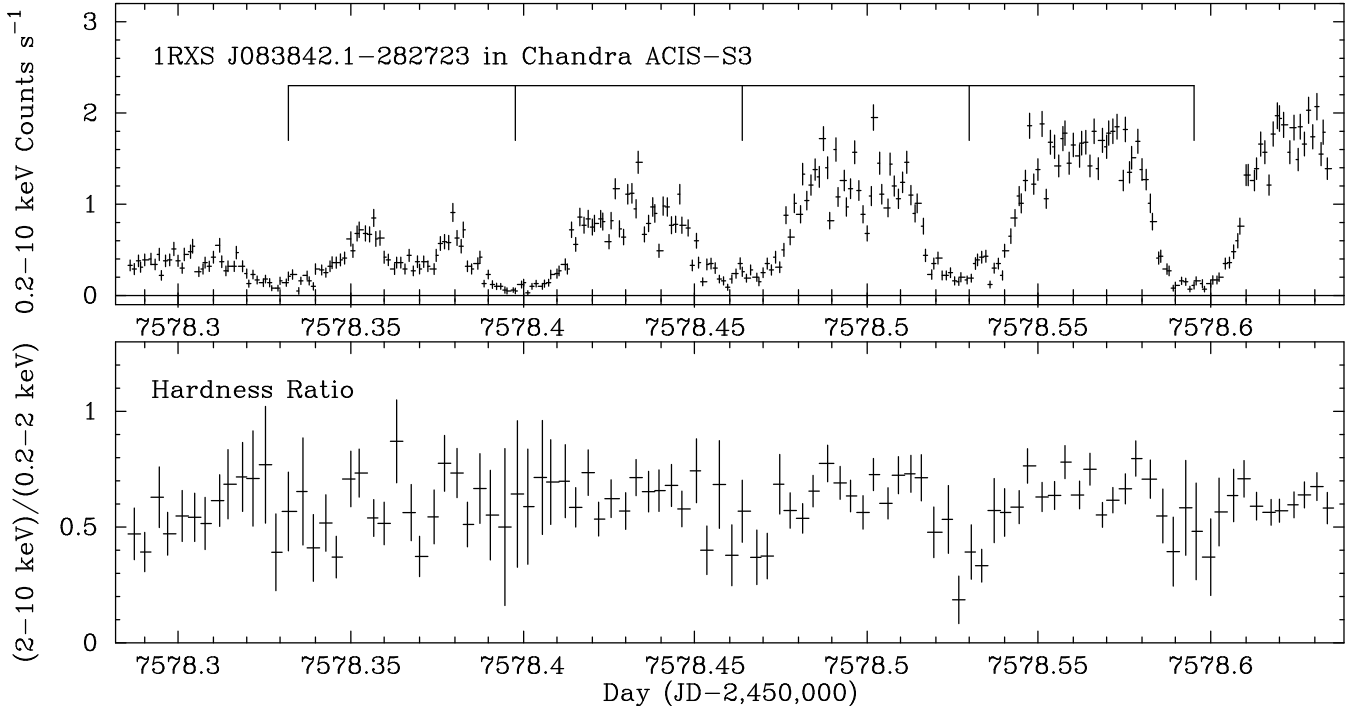


FIG. 9.— Top: Background-subtracted *Chandra* ACIS-S3 light curve of 1RXS J083842.1–282723, in 100 s bins. For comparison the tick marks are at intervals corresponding to the best-fitted period of 94.8 minutes in the *XMM-Newton* data. Bottom: Hardness ratio of counts in the (2–10 keV)/(0.2–2 keV) bands, in 300 s bins.

rival times were transformed to Barycentric Dynamical Time and extracted from a $2''$ radius around 1RXS J083842.1–282723. Figure 9 shows the 0.2–10 keV background subtracted light curve in 100 s bins. Although observation is shorter than the *XMM-Newton* ones, the behavior of 1RXS J083842.1–282723 is consistent with that observed previously. The spin period and the spin/orbit beating effect are both evident. A peak at 93.9 minutes appears in the power spectrum (Figure 8d), consistent with the *XMM-Newton* values. Since this short observation does not span a minimum of the beat cycle, it does not clearly show a phase jump in the spin cycle. However there is an “extra” dip at day 7578.37 in Figure 9 that may be due to partial pole switching of the accretion.

4. XMMU J083850.38–282756.8

Given the lack of association of any cataclysmic variable with a persistent *Fermi* γ -ray source, and the absence of a plausible physical mechanism connecting 1RXS J083842.1–282723 with 3FGL J0838.8–2829, we searched for another counterpart. In this section we describe the analysis of source “b,” XMMU J083850.38–282756.8.

4.1. *XMM-Newton* Analysis

We extracted pn light curves of XMMU J083850.38–282756.8. The MOS detectors, operated in small window mode, did not cover this source. Figure 10 shows a moderately variable light curve, and an intense flaring episode on 2015 December 2 that lasted ≈ 1.2 hr, with doubling times of ~ 100 s or less. A power-spectrum analysis, excluding the flare, does not indicate any periodicity. Upper limits on orbital

modulation in the 0.5–10 hr period range are $\sim 35\%$ for a sinusoidal amplitude. The energy spectrum of XMMU J083850.38–282756.8 is well fitted by a hard power law of photon index $\Gamma = 1.5 \pm 0.1$ (Table 4). A thermal bremsstrahlung model is also acceptable, but its temperature is very high and poorly constrained ($14.4_{-5.2}^{+11.1}$ keV). A blackbody fit is unacceptable, with reduced $\chi^2_\nu = 2.6$ and $N_H = 0$.

On December 2, the OM observed XMMU J083850.38–282756.8 for the entire span of the observation. It revealed an optical counterpart for this source that is slowly varying by ~ 1 magnitude, and has a bright maximum coincident with the X-ray flare, as shown in Figures 10 and 11. (The OM was windowed on 2015 October 20 so that it did not obtain continuous coverage of XMMU J083850.38–282756.8.)

4.2. Time-series Optical Photometry

MDM 1.3m images from 2015 February 17 and 18 are the only ones that cover this source. Because of its faintness and the short individual exposure times, we binned the images in groups of 10. Due to weather, only the 2015 February 18 observation yields a useful light curve (Figure 12). It shows a broad minimum that is characteristic of the heating light curve of a BW companion to an MSP. The X-ray and optical behavior of XMMU J083850.38–282756.8 is similar to that of BW pulsar binaries identified with *Fermi* sources, such as PSR J1311–3430, which has both optical and X-ray flares (Romani 2012). While there is only one broad minimum during the 5.4 hr span of the data, this is not necessarily a lower limit on the orbital period because of

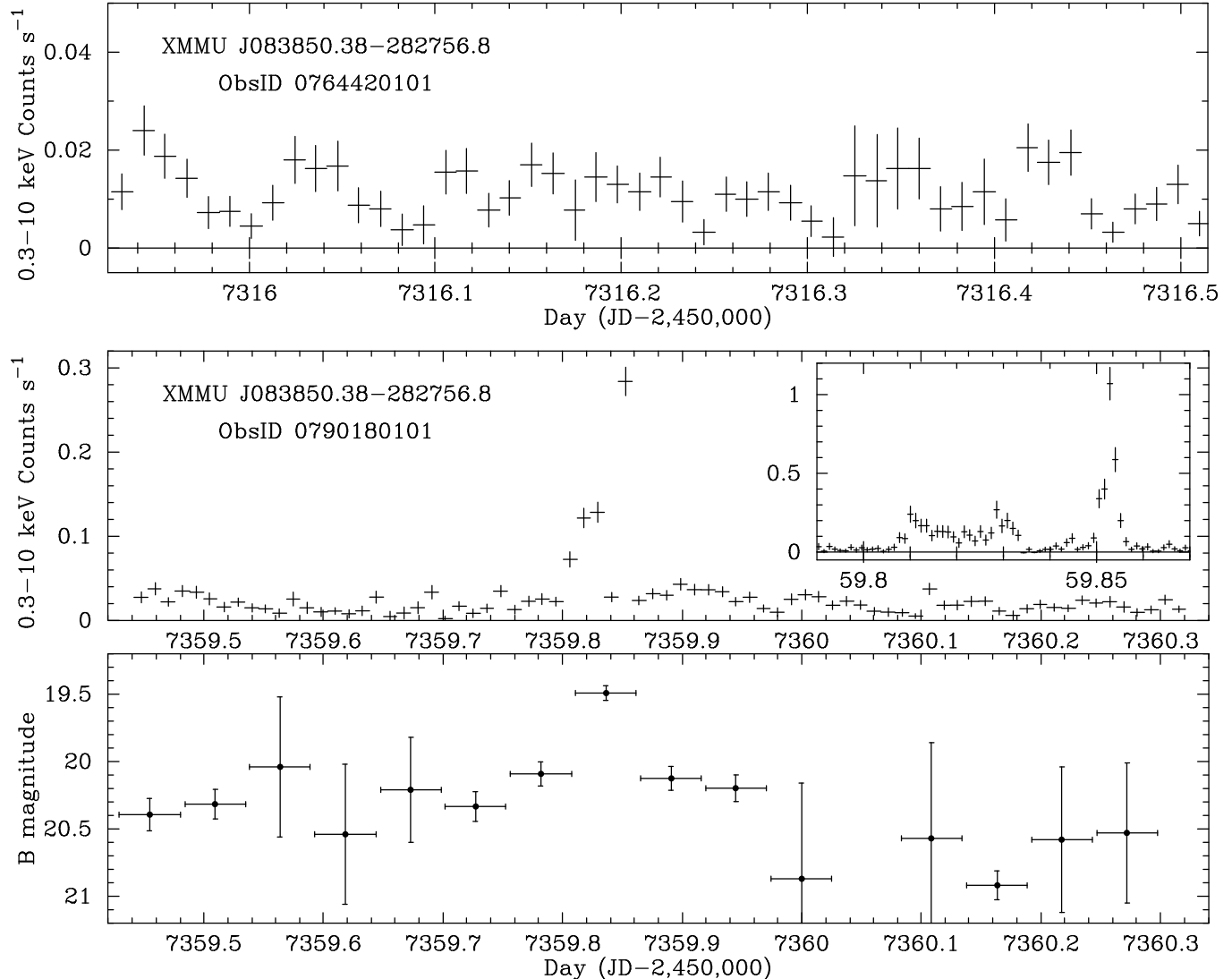


FIG. 10.— Background-subtracted *XMM-Newton* light curves of the MSP candidate XMMU J083850.38–282756.8. Top: EPIC pn 0.3–10 keV light curve in 1000 s bins on 2015 October 20 (ObsID 0764420101). Middle: EPIC pn 0.3–10 keV light curve in 1000 s bins on 2015 December 2 (ObsID 0790180101). The inset shows the 1.2 hr flaring episode at day 7359.8 at higher resolution (100 s bins). Bottom: *XMM-Newton* OM magnitudes from 4400 s exposures in *B*-band on 2015 December 2 (ObsID 0790180101). There is a gap in the data at day 7360.05.

the possibility of flaring, which may mask a second dip near the end of the time series.

5. XMMU J083842.85–282831.8

A third X-ray source on the pn CCD, XMMU J083842.85–282831.8, labeled “c” in the images of Figure 1, falls within the error circle of 3FGL J0838.8–2829. Its $\Gamma = 2.2$ power-law X-ray spectrum and relatively steady optical flux in the OM and MDM 1.3m time series (Figure 12) suggest that it is a QSO. The fitted $N_{\text{H}} = 1.26 \times 10^{21} \text{ cm}^{-2}$ is consistent with the total 21 cm $N_{\text{H}} = 1.4 \times 10^{21} \text{ cm}^{-2}$ on the line of sight (Kalberla et al. 2005). This object was also listed as a low-probability blazar candidate for 3FGL J0838.8–2829 by Massaro et al. (2013), from its colors in the *Wide-field Infrared Survey Explorer* data. Lacking a radio detection in the NVSS, it is unlikely to be a blazar. We obtained an opti-

cal spectrum of XMMU J083842.85–282831.8 using the Ohio State Multi-Object Spectrograph (OSMOS) on the MDM 2.4m telescope. In the wavelength range 3960–6880 Å it shows a single broad emission line, which we identify as Mg II $\lambda 2799$ at $z = 0.825 \pm 0.001$, with an equivalent width of ≈ 45 Å (Figure 13). This confirms that it is a non-blazar AGN, and probably unrelated to the *Fermi* source.

6. DISCUSSION

6.1. 1RXS J083842.1–282723

The X-ray light curve of 1RXS J083842.1–282723, with its deep, broad dips at a period of 94.8 ± 0.4 minutes, is typical of those polars in which self occultation of the emitting magnetic pole by the WD is responsible for the modulation. It cannot be an eclipse by the or-

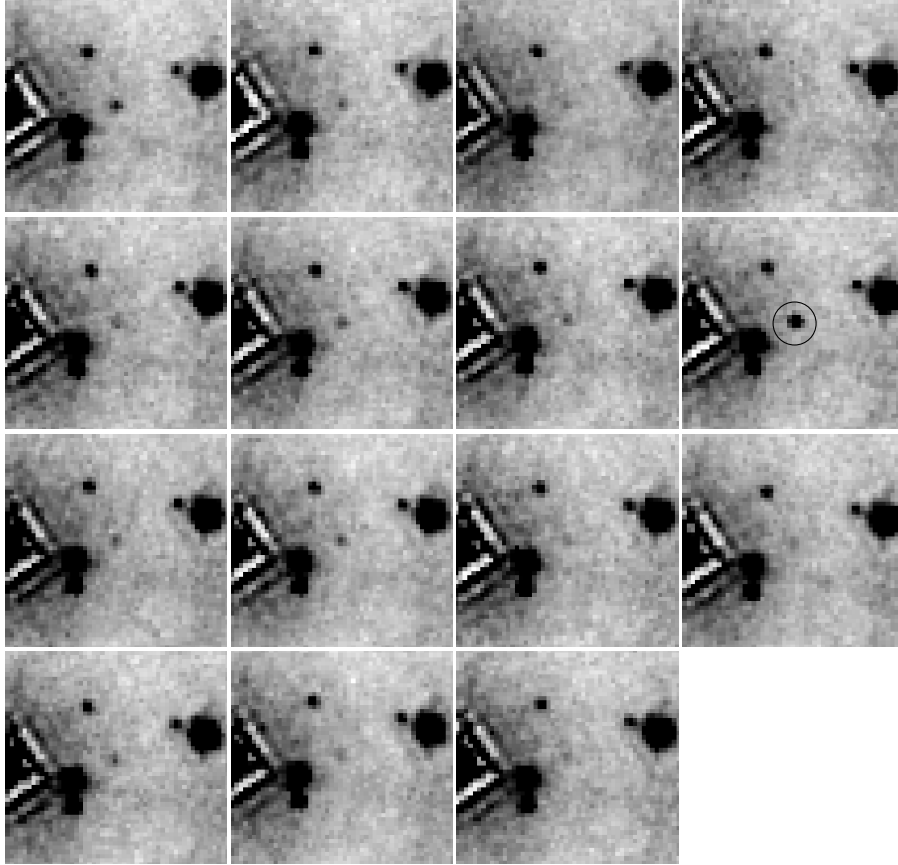


FIG. 11.— *XMM-Newton* OM *B*-filter image cutouts around the MSP candidate XMMU J083850.38–282756.8 from the 2015 December 2 observation (ObsID 079018010). Time increases from left to right and top to bottom, corresponding to the 15 points in Figure 10. The source is circled in the image coinciding with the X-ray flare. The field is $50'' \times 50''$.

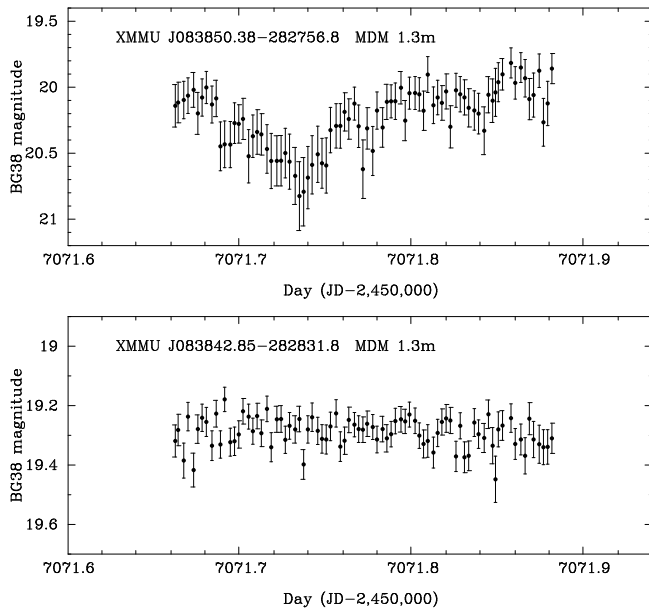


FIG. 12.— MDM 1.3m light curves of source “b” (MSP candidate XMMU J083850.38–282756.8, top) and source “c” (QSO XMMU J083842.85–282831.8, bottom), from the 2015 February 18 time series (Table 1). The 20 s images were combined in groups of 10, for an exposure time of 200 s per point.

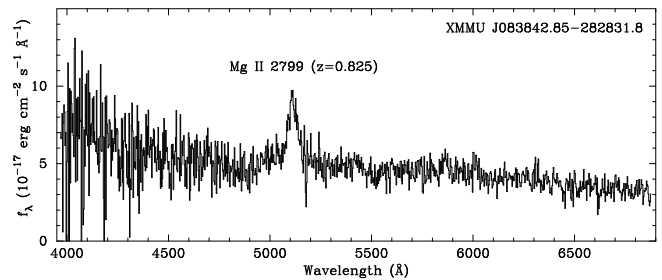


FIG. 13.— Optical spectrum of XMMU J083842.85–282831.8 from OSMOS on the MDM 2.4m telescope. The spectrum has been binned to 2.9 \AA .

biting secondary star or the accretion stream, because either of those would be much narrower. Eclipse ingress or egress of the entire WD would take only a few seconds, less than one bin of the light curves, based on the orbital velocities estimated below. The eclipse duration would be < 0.1 cycles given the radius of the secondary star. See, e.g., Worpel & Schwöpe (2015) for a light curve of an eclipsing polar.

The slower but equally deep 14.7 hr modulation requires yet another explanation. It also is too broad to be an eclipse by the orbiting secondary or accretion stream. The hardness ratio does not indicate photoelectric ab-

sorption as a cause. Instead, we hypothesize that the long period results from interruption of the accretion stream due to an orbit that is asynchronous with respect to the WD rotation. This modulates the accretion rate onto the WD with a 14.7 hr period.

In addition, the spin cycle is thrown out of phase by $\approx 120^\circ$ at the minimum of the 14.7 hr modulation. This is interpreted as switching of the accretion between not quite antipodal regions, when the accretion almost stops. The effect on the power spectrum is exactly analogous to amplitude modulation of a carrier signal, with a phase jump, which splits the signal into two periods straddling the true one. We have recovered the true period, which we interpret as the WD spin, in the three X-ray observations reported here. There is no direct manifestation of the orbit in the power spectrum, but the 14.7 hr period most likely represents the time it takes for the companion star to migrate $\approx 120^\circ$ around the WD, i.e., one-third of the beat period of the spin and the orbit. The implied orbital period is 98.3 ± 0.5 minutes, assuming that it is longer than the spin period.

The emission-line radial velocity curve has a period of 98.413 ± 0.004 minutes, which is consistent with the X-ray inferred orbital period, and not with the spin. But the radial velocity amplitude of 274 km s^{-1} is too large to be an orbital velocity of the WD, and the lines are too broad, $\sim 1500 \text{ km s}^{-1}$ to be coming from the heated face of the secondary star. A typical CV with orbital period of 100 minutes has a $0.8 M_\odot$ WD and a $0.1 M_\odot$ secondary (Savoury et al. 2011). Typical orbital velocities are then $\approx 56 \text{ km s}^{-1}$ for the WD and $\approx 445 \text{ km s}^{-1}$ for the secondary. On the other hand, free-fall velocity onto the WD is up to 3900 km s^{-1} . So we conclude that the emission lines are located high in the accretion column.

We also examined the EW of the H α emission line as a function of spectroscopic phase. The EW varies ≈ 0.5 cycles out of phase with respect to the radial velocity (Figure 2). The EW is therefore greatest at the point of maximum blueshift, phase 0.75. Assuming radial accretion, this is when the accreting pole is on the far side of the WD and maximally occulted. The emission-line source could be higher up in the accretion column than the optical continuum source, and therefore less modulated. This would result in a larger EW at phase 0.75, where the continuum is weakest.

The original group of four asynchronous polars have spin and orbit periods which periods differ by $\lesssim 2\%$ (Schwarz et al. 2007, and references therein). In 1RXS J083842.1–282723, the difference we infer is 3.7%. A fifth asynchronous polar has been proposed to explain the post-nova light curve of V4633 Sgr (Lipkin & Leibowitz 2008), which had transient period that decreased from 185.6 minutes to 183.9 minutes in addition to a stable period of 180.8 minutes. The authors attributed the longer period to the spin period, which was perturbed by the outburst, while the shorter period is orbital. It is generally observed that asynchronous polars are evolving toward synchronization on a short time scale, which suggests that nova eruptions may be the cause of all asynchronous polars.

Other CVs with more complex light curves and multiple periods have also been proposed as extreme asynchronous polars, most notably RX J0524+42, dubbed

“Paloma” (Schwarz et al. 2007; Joshi et al. 2016), and IGR J19552+0044 (Bernardini et al. 2013; Thorstensen & Halpern 2013). Paloma is suggested to have an orbital period of 157 minutes, and a spin period that is either 136 or 146 minutes, which are asynchronous by 14% or 7% respectively (Schwarz et al. 2007). IGR J19552+0044 has a spectroscopic period of 1.39 hr that disagrees with its photometric period of 1.36 hr (Thorstensen & Halpern 2013), while Bernardini et al. (2013) finds X-ray periods of 1.38 hr and 1.69 hr. For these systems with highly discrepant periods, it is not yet known if they are evolving toward synchronization, but if so, it may be for the first time. Among this group, 1RXS J083842.1–282723 has the simplest light curve and power spectrum, and thus may be a key to interpreting the other, more complex cases.

6.2. XMMU J083850.38–282756.8

None of the properties of the CV 1RXS J083842.1–282723 suggest a connection with 3FGL J0838.8–2829. Using machine learning algorithms, Mirabal et al. (2016) classified 3FGL J0838.8–2829 as a high-confidence pulsar based on its γ -ray spectral shape and variability index. Accordingly, we propose XMMU J083850.38–282756.8 as the millisecond pulsar counterpart of 3FGL J0838.8–2829.

X-ray properties of BW pulsars were reviewed by Gentile et al. (2014) and Arumugasamy et al. (2015). They have hard power-law spectra and sometimes a soft thermal component from the neutron star surface. The non-thermal emission is thought to be synchrotron from an intrabinary shock between the pulsar wind and the companion stellar wind. In some cases the X-ray flux is modulated on the orbital period, due either to relativistic beaming, or self occultation of the emitting region near the surface of the companion star (Romani & Sanchez 2016).

The optical light curves of BWs are modulated by photospheric heating. Usually the heated face of the substellar companion is much brighter than the cool photosphere on the “night” side. In some cases, the heating light curve is not symmetric with respect to the line between the stars, which could be due to an asymmetric shock, or to channeling of the pulsar wind by intrinsic magnetic fields on the companion (Tang et al. 2014; Li et al. 2014). In PSR J1311–3430, bright flares have been seen in optical and X-rays (Romani 2012), which could be coming from the companion’s magnetic fields. PSR J1311–3430 is a short-period (94 minute) system, which, being in tidally locked rapid rotation, could enhance the coronal magnetic field (Romani et al. 2015).

The hard X-ray power-law spectrum and X-ray and optical flare seen in the *XMM-Newton* observation of XMMU J083850.38–282756.8 strongly motivate its identification as the MSP counterpart of 3FGL J0838.8–2829. Typical *Fermi* MSPs are at distances of ~ 1 kpc. If so, its X-ray luminosity would be $2 \times 10^{31} \text{ erg s}^{-1}$, in the range of both BWs and redbacks in the radio pulsar state (Roberts et al. 2015). In contrast, accreting redbacks have $L_x \sim 3 \times 10^{33} \text{ erg s}^{-1}$ (Bogdanov et al. 2015).

This would be the first time that a simultaneous X-ray and optical flare is seen from a BW. It may be a short-period system similar to PSR J1311–3430, but the

X-ray light curve doesn't reveal an orbital period. Any orbital modulation in the 0.5–10 hr period range has < 35% amplitude for an assumed sinusoid. The cadence of the 4400 s OM exposures is too long to test for such a period, which may, in addition, be masked by the flaring behavior. The MDM optical data, on the other hand, have adequate cadence, and a dip that is characteristic of a heating light curve, but the dip does not repeat within the 5.4 hr time series (Figure 12), which suggests that the period is > 3.4 hr. Alternatively, a second dip may be masked by a flaring episode.

BW optical light curves are usually modulated by several magnitudes, while the dip in XMMU J083850.38–282756.8 is only ≈ 0.8 magnitudes. This could mean that the inclination angle of the binary is small, or that the companion is a low-mass main sequence star, i.e., a redback, which is brighter than a BW. Optical flares have also been seen from the redback PSR J1048+2339 (Deneva et al. 2016). Additional time-series photometry, optical spectroscopy, and a radio or γ -ray pulsar detection, could confirm the identification, and resolve the remaining questions about the basic parameters of the binary system.

7. CONCLUSIONS

The γ -ray properties of 3FGL J0838.8–2829 have suggested that it is a pulsar. In this X-ray and optical study, we first concluded that 1RXS J083842.1–282723, the brightest X-ray source in its error circle, is an unusual CV that falls there by chance. It has a simple X-ray light curve that is strongly modulated at two periods, with a phase jump that indicates pole-switching of the accretion in an asynchronous polar. The spin is manifest as a 94.8 minute X-ray period caused by self occultation of the accreting pole, while the switching interval is 14.7 hours. This implies an orbital period of 98.3 minutes, consistent with the 98.41 minute optical spectroscopic period. The strong optical and X-ray modulation on the 14.7 hr period can be explained by nearly complete interruption of the accretion stream as it switches

poles. A dedicated optical monitoring campaign could obtain a more precise value for the beat period, test the proposed geometry of the accretion spots in more detail, and determine whether the spin and orbit are evolving toward synchronism.

X-ray and optical observations identify a second, highly variable object in the error circle of 3FGL J0838.8–2829. XMMU J083850.38–282756.8 is modulated on a time scale of hours in the optical, in addition to having shown one simultaneous X-ray and optical flare. It has a hard, nonthermal X-ray spectrum. These properties are compatible with black widow or redback millisecond pulsar systems that have been discovered as counterparts of *Fermi* sources. A binary period, an important test of this hypothesis, is not yet revealed by the available data, but follow-up time-series photometry, optical spectroscopy, and/or a radio pulsar detection, should be able to determine the orbital parameters of the system.

8. ACKNOWLEDGEMENTS

We thank Eric Alper for obtaining time-series photometry of 1RXS J083842.1–282723 in 2016 March, and Jessica Klusmeyer for the optical spectrum of the QSO XMMU J083842.85–282831.8. The MDM Observatory is operated by Dartmouth College, Columbia University, the Ohio State University, Ohio University, and the University of Michigan. The results reported in this article are based in part on observations made by the *Chandra* X-ray Observatory. Support for this work was provided by the National Aeronautics and Space Administration through *Chandra* Award Number SAO GO6-17027X issued by the *Chandra* X-ray Observatory Center, which is operated by the Smithsonian Astrophysical Observatory for and on behalf of the National Aeronautics Space Administration under contract NAS8-03060. This investigation also uses observations obtained with *XMM-Newton*, an ESA science mission with instruments and contributions directly funded by ESA Member States and NASA.

REFERENCES

- Acero, F., Ackermann, M., Ajello, M., et al. 2015, *ApJS*, 224, 8
 Archibald, A. M., Stairs, I. H., Ransom, S. M., et al. 2009, *Science*, 324, 1411
 Arumugasamy, P., Pavlov, G. G., & Garmire, G. P. 2015, *ApJ*, 814, 90
 Bassa, C. G., Patruno, A., Hessels, J. W. T., et al. 2014, *MNRAS*, 441, 1825
 Bernardini, F., de Martino, D., Mukai, K., et al. 2013, *MNRAS*, 435, 2822
 Bogdanov, S., Archibald, A. M., Bassa, C., et al. 2015 *ApJ*, 806, 148
 Bogdanov, S., & Halpern, J. P. 2015, *ApJL*, 803, L27
 Bond, H. E., White, R. L., Becker, R. H., & O'Brien, M. S. 2002, *PASP*, 114, 1359
 Butters, O. W., Norton, A. J., Hakala, P., Mukai, K., & Barlow, E. J. 2008, *A&A*, 487, 271
 de Martino, D., Belloni, T., Falanga, M., et al. 2013, *A&A*, 550, A89
 Deneva, J. S., Ray, P. S., Camilo, F., et al. 2016, *ApJ*, 823, 105
 Gentile, P. A., Roberts, M. S. E., McLaughlin, M. A., et al. 2014, *ApJ*, 783, 69
 Halpern, J. P., & Thorstensen, J. R. 2015, *AJ*, 150, 170
 Joshi, A., Pandey, J. C., Singh, K. P., & Agrawal, P. C. 2016, *ApJ*, 830, 56
 Kalberla, P. M. W., Burton, W. B., Hartmann, D., et al. 2005, *A&A*, 440, 775
 Li, M., Halpern, J. P., & Thorstensen, J. R. 2014, *ApJ*, 795, 115
 Lipkin, Y. M., & Leibowitz, E. M. 2008, *MNRAS*, 387, 289
 Masetti, N., Morelli, L., Palazzi, E., et al. 2006, *A&A*, 459, 21
 Masetti, N., Sbarufatti, B., Parisi, P., et al. 2013, *A&A*, 559, A58
 Massaro, F., D'Abrusco, R., Paggi, A., et al. 2013, *ApJS*, 206, 13
 Mirabal, N., Charles, E., Ferrara, E. C., et al. 2016, *ApJ*, 825, 69
 Papitto, A., Ferrigno, C., Bozzo, E., et al. 2013, *Nature*, 501, 517
 Roberts, M. S. E. 2013, in *Proc. IAU Symp.* 291, *Neutron Stars and Pulsars: Challenges and Opportunities after 80 years*, ed. J. van Leeuwen (Cambridge: Cambridge Univ. Press), 127
 Roberts, M. S. E., McLaughlin, M. A., Gentile, P. A., et al. 2015, in *Fifth Int. Fermi Symp. Proc.* (arXiv:1502.07208)
 Romani, R. W. 2012, *ApJL*, 754, L25
 Romani, R. W., Filippenko, A. V., & Cenko, S. B. 2015, *ApJ*, 804, 115
 Romani, R. W., & Sanchez, N. 2016, *ApJ*, 828, 7
 Roy, J., Ray, P. S., Bhattacharyya, B., et al. 2015, *ApJL*, 800, L12
 Savoury, C. D. J., Littlefair, S. P., Dhillon, V. S., et al. 2011, *MNRAS*, 415, 2025
 Schwarz, R., Schwope, A. D., Staude, A., et al. 2007, *A&A*, 473, 511
 Tang, S., Kaplan, D. L., Phinney, E. S., et al. 2014, *ApJL*, 791, 5
 Thorstensen, J. R., & Armstrong, E. 2005, *ApJ*, 130, 759
 Thorstensen, J. R., & Halpern, J. 2013, *AJ*, 146, 107
 Wickramasinghe, D. T. 1989, in *Proc. IAU Colloq.* 114, *White Dwarfs*, ed. G. Wegner (Berlin: Springer), 314
 Worpel, H., & Schwope, A. D. 2015, *A&A*, 583, A130
 Zacharias, N., Finch, C. T., Girard, T. M., et al. 2013, *AJ*, 145, 44